

May 2023

## Joint Constraints on Kepler-36 from Kepler and New KECK-HIRES Data

Nicholas Juliano

Follow this and additional works at: <https://digitalscholarship.unlv.edu/thesesdissertations>



Part of the [Astrophysics and Astronomy Commons](#), and the [Other Physics Commons](#)

---

### Repository Citation

Juliano, Nicholas, "Joint Constraints on Kepler-36 from Kepler and New KECK-HIRES Data" (2023). *UNLV Theses, Dissertations, Professional Papers, and Capstones*. 4718.  
<http://dx.doi.org/10.34917/36114743>

This Thesis is protected by copyright and/or related rights. It has been brought to you by Digital Scholarship@UNLV with permission from the rights-holder(s). You are free to use this Thesis in any way that is permitted by the copyright and related rights legislation that applies to your use. For other uses you need to obtain permission from the rights-holder(s) directly, unless additional rights are indicated by a Creative Commons license in the record and/or on the work itself.

This Thesis has been accepted for inclusion in UNLV Theses, Dissertations, Professional Papers, and Capstones by an authorized administrator of Digital Scholarship@UNLV. For more information, please contact [digitalscholarship@unlv.edu](mailto:digitalscholarship@unlv.edu).

# JOINT CONSTRAINTS ON KEPLER-36 FROM KEPLER AND NEW KECK-HIRES DATA

By

Nicholas J. Juliano

Bachelor of Science – Physics  
University of New York at Oneonta  
2011

A thesis submitted in partial fulfillment  
of the requirements for the

Master of Science – Astronomy

Department of Physics and Astronomy  
College of Sciences  
The Graduate College

University of Nevada, Las Vegas  
May 2023



## Thesis Approval

The Graduate College  
The University of Nevada, Las Vegas

Date

This thesis prepared by

Nicholas Juliano

entitled

Joint Constraints on Kepler-36 from Kepler and New KECK-HIRES Data

is approved in partial fulfillment of the requirements for the degree of

Master of Science - Astronomy  
Department of Physics and Astronomy

Jason Steffen  
*Examination Committee Chair*

Zhaohuan Zhu  
*Examination Committee Member*

Rebecca Martin  
*Examination Committee Member*

Elisabeth Hausrath  
*Graduate College Faculty Representative*

Alyssa Crittenden, Ph.D.  
*Vice Provost for Graduate Education &  
Dean of the Graduate College*

## ABSTRACT

I analyze new HIRES Radial Velocity (RV) data in conjunction with transit mid-times and uncertainties from the full 17 quarters of Kepler data to reassess the orbital parameters of the Kepler-36 system. Six additional RV measurements were taken by the Keck-HIRES spectrograph from September 21, 2021 to October 11, 2021. I carry out a differential evolution Markov Chain Monte Carlo-based (DEMCMC) analysis to infer improved orbital elements for the two known planets in the system. Leveraging additional information provided by the new RV measurements, I extend this DEMCMC analysis to a possible three-planet configuration. I explore the likelihood of a third planet using common statistical tests as comparison tools for my fitted two-planet and three-planet models of the Kepler-36 system. My analysis favors a three-planet model containing a previously-undetected planet with a mass of an orbital period near 43 Earth-masses and an orbital period near 170 days. Should future observations of this system further support the presence of this third planet, it will place significant constraints on the formation and dynamical evolution of this system—which produced the inner planet pair in such close proximity to each other, with a period ratio near 7:6.

To my wife, Sabrina, for remaining my greatest discovery.

## TABLE OF CONTENTS

ABSTRACT .....	iii
LIST OF TABLES .....	vi
LIST OF FIGURES .....	vii
CHAPTER 1 INTRODUCTION.....	1
CHAPTER 2 BACKGROUND .....	3
CHAPTER 3 DATA .....	5
CHAPTER 4 METHODS .....	8
4.1 Priors and Initializations .....	9
4.1.1 Priors for the Known Planets .....	9
4.1.2 Priors for the Possible Third Planet .....	10
CHAPTER 5 RESULTS .....	15
5.1 Posteriors .....	15
5.2 Statistical Analysis .....	20
CHAPTER 6 DISCUSSION .....	22
REFERENCES .....	24
CURRICULUM VITAE .....	27

## LIST OF TABLES

3.1	HIRES measurements of the Kepler-36 system .....	6
4.1	The prior distributions of each orbital element in my simulations. All elements with a single value are fixed. Bracketed elements indicate the minimum and maximum values of flat prior distributions. ....	11
4.2	Posterior maximum likelihood .....	11
5.1	The standard deviation of the posterior distribution of each parameter in the two-planet fit .....	19
5.2	The standard deviation of the posterior distribution of each parameter in the three-planet fit .....	19
5.3	Statistical test results .....	21

## LIST OF FIGURES

3.1	a) The radial velocity of Kepler-36 induced by both Kepler-36 b and Kepler-36. b) Residuals of the radial velocity induced by Kepler-36 b and Kepler-36 c. c) The phase-folded radial velocity of Kepler-36 induced by Kepler-36 b. Red points indicate binned data with a bin size of 0.1 d) The phase-folded radial velocity of Kepler-36 induced by Kepler-36 c .....	7
4.1	Combined posterior of all free parameters for the two-planet fit. The dark and gray circles indicate the 68.3% and 95.5% confidence regions, respectively. ....	12
4.2	Combined posterior of all free parameters for the three-planet fit. The dark and gray circles indicate the 68.3% and 95.5% confidence regions, respectively. ....	13
4.3	Transit timing variations (blue dots) for planets in the Kepler-36 system compared to the best fit (solid lines) obtained using the full <i>Kepler</i> data set .....	14
5.1	Radial velocity simulations of Kepler-36 induced by each of my best-fit models. Observations are shown as blue dots. Residuals are shown in the lower panel. ....	17
5.2	The Lomb-Scargle periodogram of the residuals of the RV data as simulated by the posterior maximum likelihood orbital elements of the two-planet fit. The yellow line denotes the false alarm probability.....	18



## CHAPTER 1 INTRODUCTION

Through a combination of precise photometric measurements and the extension of the transit method to that of transit timing variations (TTVs), the Kepler space telescope’s four-year period of stellar observation has led to the discovery of thousands of planets and planetary candidates (Coughlin et al. (2015), Morton et al. (2016)). While this mission had particular success detecting planets with short orbital periods of  $<\sim 1\text{yr}$ , its limited duration establishes an inherent difficulty when attempting to detect orbiting planets with longer periods. Additionally, photometric observations like those made by Kepler are poor at detecting non-transiting, inclined planets. A common approach to further understand planetary systems observed by Kepler is to follow up on these observations with radial velocity (RV) measurements. Here I report on such a follow up performed on the Kepler-36 system.

Initially discovered in Carter et al. (2012), the known Kepler-36 system consists of a sub-giant star of near-solar mass and two transiting planets. Kepler-36b and Kepler-36c are known to have masses on the order of magnitude of the Earth ( $m_b \sim 4M_{\oplus}$  and  $m_c \sim 7M_{\oplus}$ ) (Vissapragada et al. 2019) and orbit closely to their host star with a period ratio near 7:6. Adding to the uniqueness of this planetary system is the proximity of the planets’ orbits and their vastly different densities. The two planets have semi-major axes that differ by only 10.29%, yet their densities are 6.8 and  $0.86\text{ g/cm}^3$ , respectively. Because of these anomalous properties, the characteristics of this planetary system have been exhaustively studied over the years (Lopez & Fortney 2013; Quillen et al. 2013; Bodenheimer et al. 2018; Agol & Carter 2019). However, spectroscopic observations of

the host star reveal additional RV activity in this system unaccounted by the known planets. This demonstrates a need to explore the possibility of additional bodies orbiting the host star.

This paper is structured as follows. In chapter 2 I highlight some historical research on the Kepler-36 system. In chapter 3 I describe the data I use. In chapter 4 I detail the methods I used to perform my analysis. In chapter 5 I compare the empirical results of my two-planet and three-planet models. I also use statistical tests to explore the possibility of a third planet in the Kepler-36 system. Finally, in chapter 6, I provide direction for future research on the Kepler-36 system and speculate on the consequences of my results.

## CHAPTER 2 BACKGROUND

As discussed previously, several attributes contribute to the anomalous and intriguing nature of the Kepler-36 system and make analyses of this system a useful proxy for identifying edge cases of planetary formation and evolution theories. Since its discovery in 2012, there have been several such analyses.

The physical separation of the two known planets is remarkably small at approximately 0.1 (Carter et al. 2012). This was the smallest fractional separation of all known multiplanet systems. Of complementary remarkableness was that it had one of the largest known density contrasts ( $\sim 8:1$ ). The masses and radii were constrained in Deck et al. (2012) from transit timing variations with consideration given to the system's long-term orbital stability. The high precision of these values furthered the utility of this system for theoretical analysis.

A logical supposition to explain this unique configuration is that the two planets formed at widely separated locations and migrated into close proximity. This was first explored in Deck et al. (2012). Specifically, this work explored a convergent migration model, where both planets formed in locations other than their current locations and subsequently migrated until they locked into their current approximate 6:7 orbital resonance.

Quillen et al. (2013) further explored a migration explanation by fine-tuning several initial conditions in an attempt to allow two convergently migration planets to bypass other mean motion resonances and to arrive at 7:6. When considering embryos comparable to Mars in size, they found that gravitational interactions are sufficient to allow the embryos to escape resonances. They

further provided support for a convergent migration model by accounting for proximity and density contrast through a series of collisions and these gravitational interactions.

Around this time, more works provided complementary insight on how such a planetary configuration could be possible. For example, Paardekooper et al. (2013) demonstrated that configurations involving close proximity and wide density variations can occur given a wide range of migration parameters in a turbulent protoplanetary disc. Additionally, to explain the density variation, Lopez & Fortney (2013) explored the system from the perspective of thermal evolution and photo-evaporative mass loss. They found that photo-evaporation coupled with slight differences in the planets' mass-iron cores could explain this density variation.

Subsequent formation models considered alternate initial conditions and configurations. Bodenheimer et al. (2018) considered the formation models identified to-date and explored multiple configurations in which one or both of the known planets formed in situ. This work was somewhat inconclusive as it was able to find agreement with the present-day configuration of the Kepler-36 system with Kepler-36 b forming in situ and Kepler-36 c forming either in situ or migrating to its current state.

While several attempts have been made to explain the formation of this system, none have been able to confidently or conclusively identify a sole viable explanation. In other words, this problem is still unsolved. As expected, formation models have yet to account for a third planet in the Kepler-36 system.

## CHAPTER 3 DATA

While the Kepler space telescope provides precise photometric measurements, I adopted the reduced data published in Rowe et al. (2015), which distilled this photometry into transit parameters. This provides us with a straightforward way of simulating transits and TTVs while avoiding computational complexity associated with photodynamical simulations, which instead seek to simulate the full light curve of a model. For simulation purposes, the only transit parameters I needed to consider were the transit midpoints associated with each known planet in the Kepler-36 system.

The RV data for this work was collected using the High Resolution Echelle Spectrometer (HIRES) at the Keck Observatory, which has the ability to achieve precise Doppler measurements with an RMS of  $\sim 2\text{ms}^{-1}$ . Between July 30, 2012 and October 2, 2021, for a total of 25 Doppler measurements were taken by HIRES of the Kepler-36 system.

The RV data is listed in table 3.1. Figure 3.1 shows this data alongside simulations using the two-planet Kepler-36 model as constrained by TTVs alone in Hadden & Lithwick (2017). The residuals demonstrate that an RV-based approach to analyzing the Kepler-36 system specifically is particularly interesting. Despite being well constrained by transit and TTV methods, the known bodies in this system poorly describe the radial velocity observed by HIRES. This indicates more activity than models based on Kepler data alone can account for. Furthermore, the Kepler-36 system has not yet been followed up with RV approaches.

Table 3.1: HIRES measurements of the Kepler-36 system

BJD ( - 2454900.0)	RV (m/s)	unc. RV (m/s)
1238.960111	12.40	3.22
1302.747190	-14.60	4.40
1980.986613	-3.48	4.04
1992.948262	-4.74	3.29
2009.872368	-4.73	3.25
2012.827319	-2.00	3.48
2251.077157	5.94	3.55
2280.097595	-0.43	3.53
2308.096426	9.77	3.71
2332.984981	-5.47	3.42
2343.082964	-13.49	4.02
3394.878483	6.24	3.32
3422.919588	-0.95	4.99
3429.871325	9.99	3.53
3437.067316	-8.30	3.83
3483.960506	1.59	4.13
3491.919851	7.80	3.76
3495.857491	8.38	3.60
3823.006589	3.68	3.58
4578.904109	4.31	3.67
4581.905374	-0.04	3.54
4584.862818	-0.40	3.38
4589.803662	-18.80	3.68
4597.749138	-5.08	3.40
4598.867840	8.90	3.41

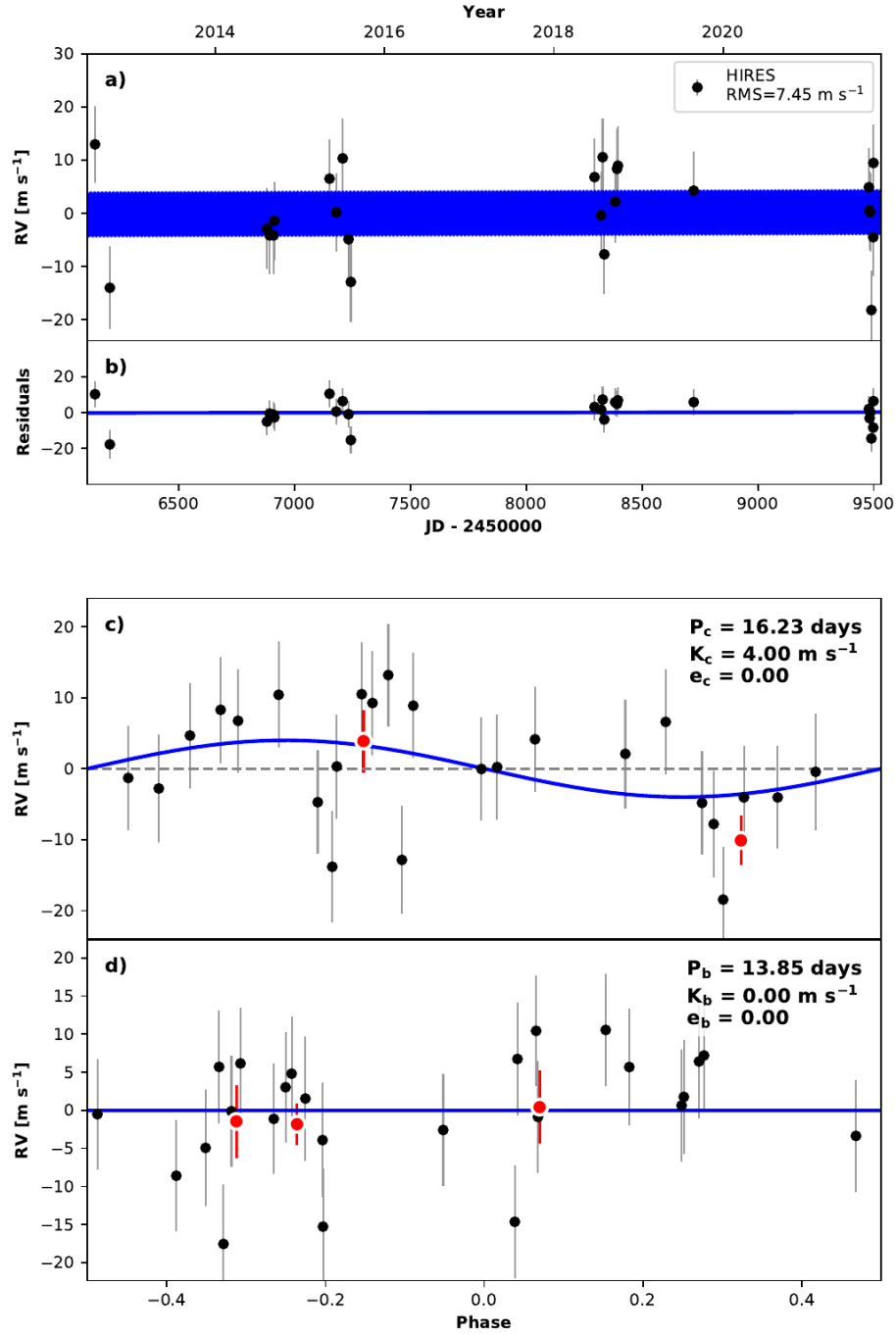


Figure 3.1: a) The radial velocity of Kepler-36 induced by both Kepler-36 b and Kepler-36. b) Residuals of the radial velocity induced by Kepler-36 b and Kepler-36 c. c) The phase-folded radial velocity of Kepler-36 induced by Kepler-36 b. Red points indicate binned data with a bin size of 0.1 d) The phase-folded radial velocity of Kepler-36 induced by Kepler-36 c

## CHAPTER 4 METHODS

I conducted a joint fit of TTV and RV data to determine posterior probability distributions of orbital elements in the Kepler-36 system with the Differential Evolution Monte Carlo Markov Chain Algorithm (DEMCMC) of Braak (2006) as implemented in the *emcee* code (Foreman-Mackey et al. 2012). I fit the currently accepted two-planet model and one including an additional orbiting body.

I performed simulations of transit mid-point times and radial velocity within this DEMCMC fit using TTVFast (Deck et al. 2014) due to its ability to accurately simulate both measurements simultaneously at minimal computational cost. ter Braak & Vrugt (2008) showed that a snooker updater improves the practical applicability of DEMCMC as free parameter count increases. Because the relatively large number of free parameters in my model, I opted to include a snooker updater in a random 10% of my steps.

I did not consider models using either data source individually because transit-only fits are already well described in Rowe et al. (2015) and Jontof-Hutter et al. (2021). Additionally, the HIRES measurements are not evenly sampled enough to fit independently. As such, I generated two models, one describing a two-planet system and one describing a three-planet system. These were generated using the approach outlined above, where both of these models considered RV and TTV data simultaneously.



## 4.1 Priors and Initializations

For each fit, the number of parallel DEMCMC chains were set to be three times the number of free parameters. Possible free parameters for consideration when performing DEMCMC runs of this nature include all Keplerian orbital elements. To reduce the computational cost of my DEMCMC runs, and because mutual inclinations of planets can be large and still be well described by coplanar TTVs (Nesvorny & Vokrouhlicky 2014), I kept inclination and longitude of ascending node fixed. This left the free parameters as planetary mass  $m_i$ , the orbital period  $P_i$ , the eccentricity  $e_i$ , the argument of periastron  $\omega_i$ , and the mean anomaly  $M_{0,i}$ . The subscript  $i$  denotes the  $i$ th planet,  $i = b, c$ . I kept the central stellar mass fixed to  $M_\star = 1.034M_\odot$  as in Yoffe et al. (2020). The prior distributions of the free parameters are outlined in Table 4.1. I initialized free parameters with flat prior distributions bound by physical constraints or previous studies as detailed below.

### 4.1.1 Priors for the Known Planets

For the two known planets, I constrained the orbital parameters as follows:  $m$  randomly distributed between 0 and  $10 M_\oplus$  based on previous studies (Carter et al. 2012; Hadden & Lithwick 2017);  $P$  randomly distributed between  $P_{0,i}-0.05$  day and  $P_{0,i}+0.05$  day, where  $P_{0,i}$  is the period provided in Rowe et al. (2015) of planet  $i$  and the  $\pm 0.05$  day range is generously several orders of magnitude larger than the errors;  $e$  randomly distributed between 0 and 0.04, since eccentricities  $e > 0.04$  are likely to induce instability and Carter et al. (2012) showed that  $e_i < 0.04$ ; and  $\omega$  and  $M$  randomly distributed between 0 and  $360^\circ$ .

### 4.1.2 Priors for the Possible Third Planet

I kept some orbital parameters fixed to reduce model complexity and reduce computational cost. For example, I only considered third planets with circular orbits, fixing  $e_d$  to 0. This assumption is necessary given the temporal inconsistency of the RV measurements. Additionally, I kept  $i_d$  and  $\Omega_d$  fixed for the same reasons described in the previous section.

My approach to the remaining free parameters,  $m_d$ ,  $P_d$ , and  $M_d$ , was to allow generous exploration of parameter space. To fulfill this objective I chose uninformative priors that sampled a realistic parameter space for these orbital elements. This eliminated the risk of prior expectations adulterating the posterior distribution of the analysis. The mean anomaly was permitted to explore its entire domain. I constrained mass to a generously large parameter space, where values above and below my limits are not physically reasonable explanations for my observations.

My constraints on orbital period,  $P_d$ , were considered carefully. I first sought to rely on the Lomb-Scargle periodogram of RV of Kepler-36 as induced by the posterior maximum likelihood orbital elements of the two-planet model as demonstrated in Figure 5.2 and discussed in more detail in subsequent sections. This periodogram demonstrated a convincingly high power peak at  $\sim 173$  days with a correspondingly low false alarm probability. However, Earth's orbit is sometimes observed as an alias of long-period power, and this peak is close to half of the Earth's orbit. Because of this, I opted to broaden my priors to the generously large  $40 \leq P_d \leq 600$  range.

Table 4.1: The prior distributions of each orbital element in my simulations. All elements with a single value are fixed. Bracketed elements indicate the minimum and maximum values of flat prior distributions.

Orbital Element	Kepler-36b	Kepler-36c	Kepler-36d
Mass	$[1, 10] M_{\oplus}$	$[1, 10] M_{\oplus}$	$[1, 400] M_{\oplus}$
Period	$[13.799, 13.899] d$	$[16.1869, 16.2869] d$	$[40, 600] d$
Eccentricity	$[0.00, 0.04]$	$[0.00, 0.04]$	0.00
Inclination	$90.0^{\circ}$	$90.0^{\circ}$	$90.0^{\circ}$
Asc. Node	$0.0^{\circ}$	$0.0^{\circ}$	$0.0^{\circ}$
Arg. of Peri.	$[0.0, 360.0]^{\circ}$	$[0.0, 360.0]^{\circ}$	$0.0^{\circ}$
Mean Anom.	$[0.0, 360.0]^{\circ}$	$[0.0, 360.0]^{\circ}$	$[0.0, 360.0]^{\circ}$

Table 4.2: Posterior maximum likelihood

Planet	Orbital Element	Two-Planet Run	Three-Planet Run
Kepler-36b	Mass	4.4086	4.4079
	Period	13.8391	13.8390
	Eccentricity	0.0259	0.0284
	Inclination	90.0	90.0
	Asc. Node	0.0	0.0
	Arg. of Peri.	81.4525	89.5704
	Mean Anom.	228.9649	221.2440
Kepler-36c	Mass	7.5012	7.4782
	Period	16.2401	16.2402
	Eccentricity	0.0004	0.0036
	Inclination	90.0	90.0
	Asc. Node	0.0	0.0
	Arg. of Peri.	304.1220	144.9822
	Mean Anom.	139.3242	298.8267
Kepler-36d	Mass	-	42.9010
	Period	-	173.5355
	Eccentricity	-	0.0
	Inclination	-	90.0
	Asc. Node	-	0.0
	Arg. of Peri.	-	0.0
	Mean Anom.	-	93.0557

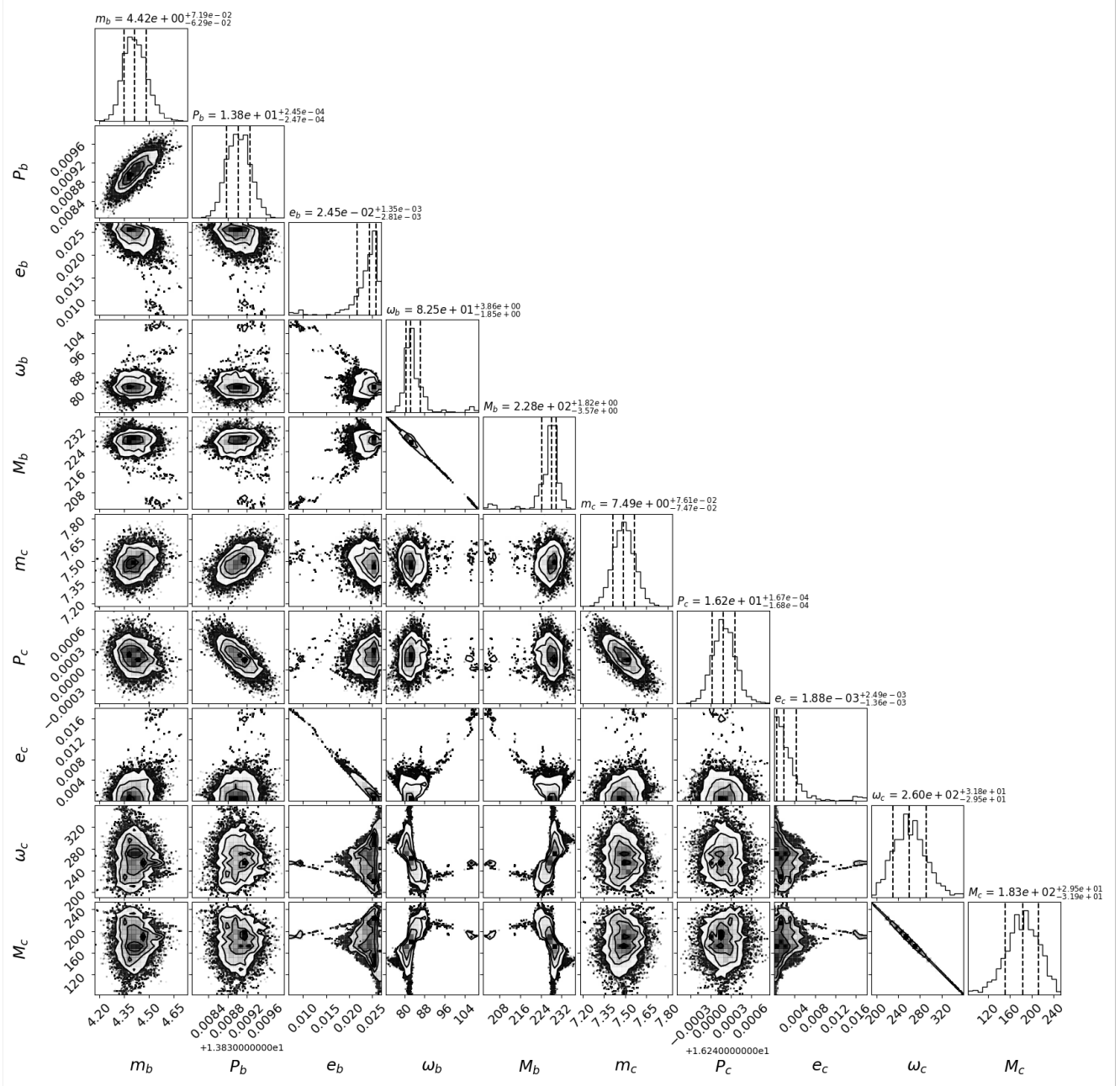


Figure 4.1: Combined posterior of all free parameters for the two-planet fit. The dark and gray circles indicate the 68.3% and 95.5% confidence regions, respectively.

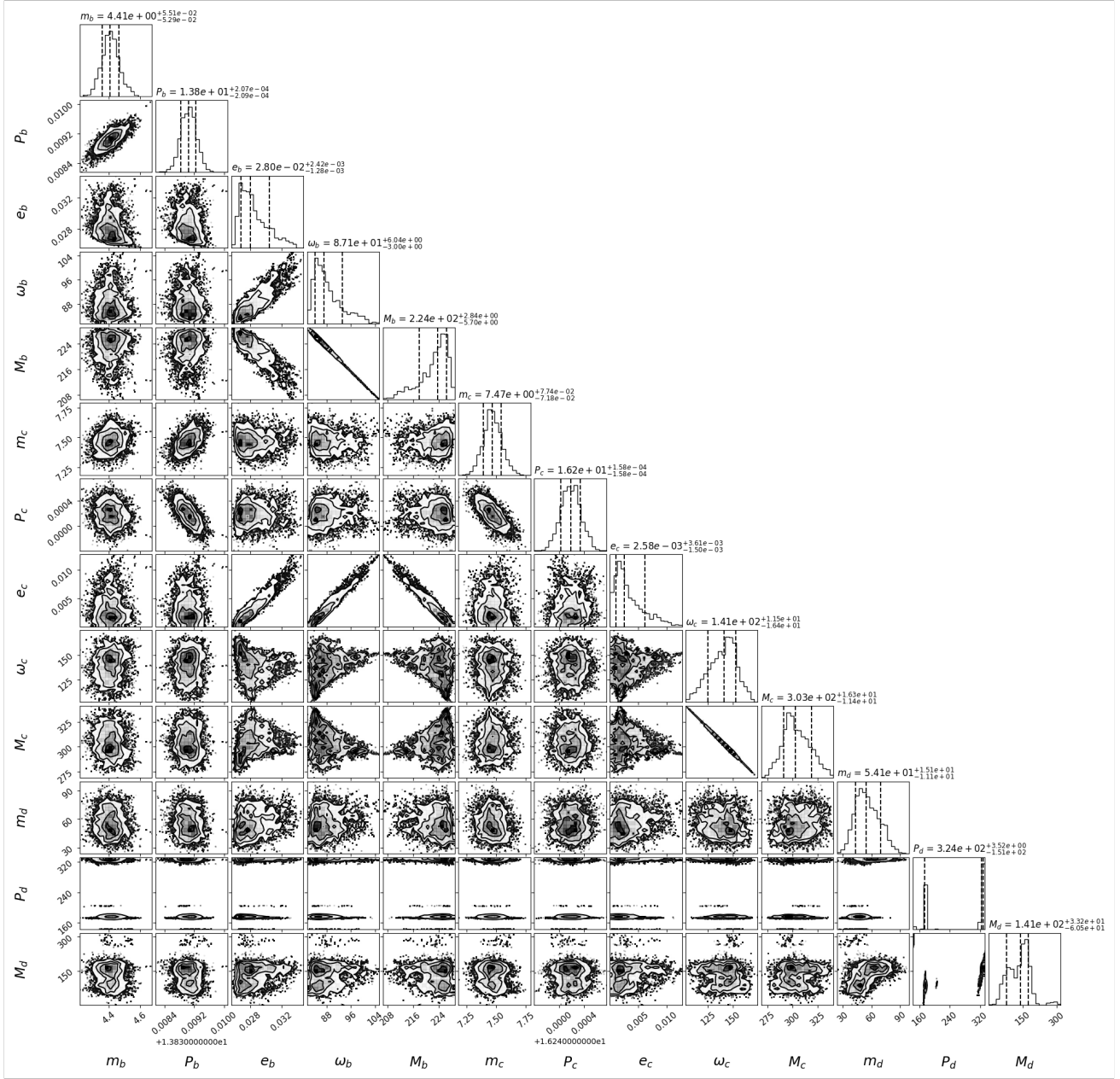


Figure 4.2: Combined posterior of all free parameters for the three-planet fit. The dark and gray circles indicate the 68.3% and 95.5% confidence regions, respectively.

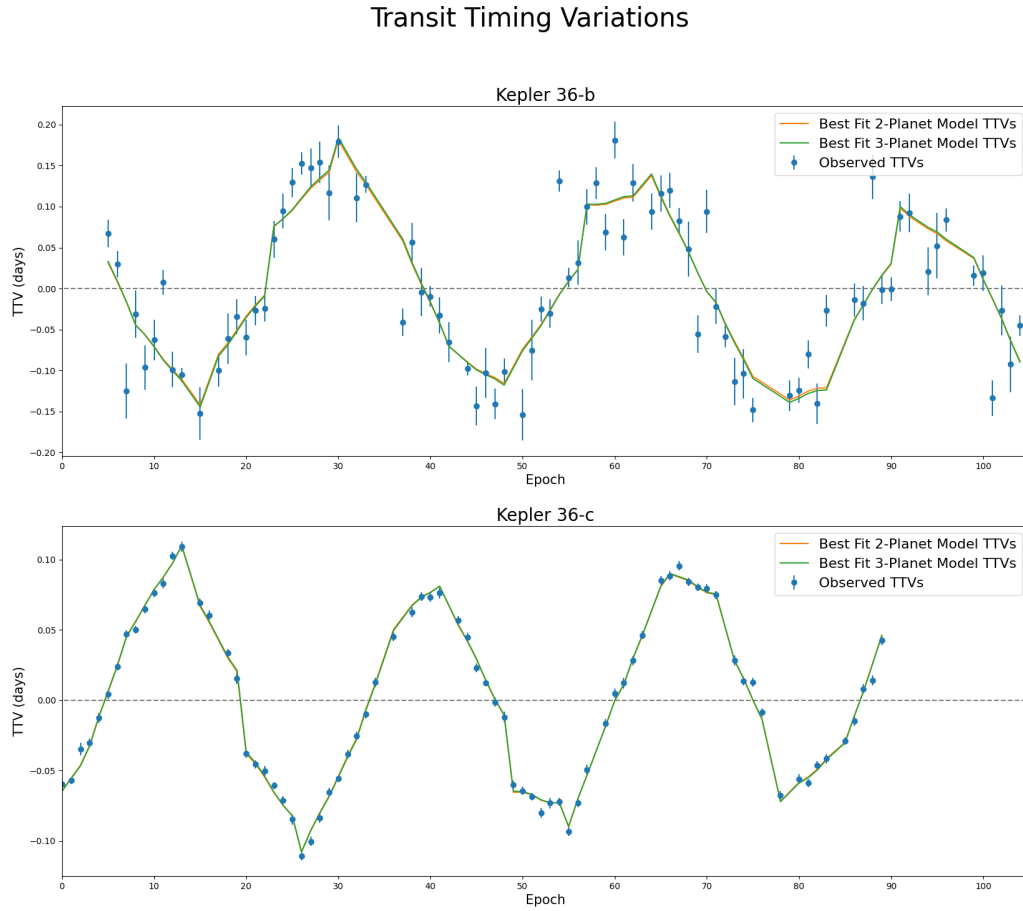


Figure 4.3: Transit timing variations (blue dots) for planets in the Kepler-36 system compared to the best fit (solid lines) obtained using the full *Kepler* data set

## CHAPTER 5 RESULTS

### 5.1 Posteriors

I performed 8,580,000 total DEMCMC iterations for the two-planet fit, and 4,630,000 total iterations for the three-planet fit. The resulting covariance plots are shown in Figure 4.1 and Figure 4.2, respectively. The best-fit orbital elements, those with the highest likelihood, for each DEMCMC run are included in Table 4.2.

As recommended by the emcee code, I considered the stopping criteria of sufficiently large autocorrelation as outlined in Goodman & Weare (2010). Specifically, I set a stopping criterion of 50 autocorrelation lengths. However, estimating integrated autocorrelation time proved to be ineffective. At most, I achieved  $\sim 4.4$  autocorrelation lengths. It is possible that this may be attributed to the multi-modality of angular orbital element configurations. Another metric, the Gelman-Rubin statistic (Gelman & Rubin 1992), is widely considered to be a standard convergence assessment tool. That said, Gelman-Rubin statistic is not practical for this work as the chains in my fits are not independently sampled (a requirement for this approach).

Noting that it is never formally possible to guarantee convergence and any attempts to do so will be heuristic in nature, I opted to run my fits for as long as my computational resources would permit and instead assess the convergence of my fits by considering the confidence interval of the posterior distribution of each parameter and comparing it to the range of the prior distribution. As shown in table 5.1 and table 5.2, the standard deviation of every posterior distribution collapsed to an average of 2.93% of its prior distribution for the two-planet system and 4.3% for the three-planet

system.

The two-planet covariance plot demonstrates reasonably well-constrained posteriors. Additionally, comparing the best-fit orbital elements for both simulations shows that including the third planet has little influence on the parameter distribution of the inner two planets. This highlights that previous efforts to constrain the Kepler-36 system that consider only two planets are consistent with this effort to identify a potential additional body. The two known planets fit well to transit timing variations, do very little to explain my RV measurements, and are relatively unaffected by the inclusion of a longer period, higher mass body.

The bi-modality of the three-planet fit as observed in  $P_d$  and  $M_d$  is to be expected. The standard deviation of  $P_d$  in this posterior distribution is shown to be quite wide due to this bi-modality. This width propagates to the magnitude of the corresponding calculations shown in table 5.2. However, it is visually apparent on the posterior covariance plot for the three-planet fit that there are two distinguishable and separate peaks for the posteriors of  $P_d$  at approximately 173 days and 346 days.

While it is apparent that the peak for  $P_d$  at approximately 346 days is higher than that of approximately 173 days, the model using the 173 day value resulted in a higher probability. This discrepancy is understood when considering the domain of the uninformative prior of  $P_d$  in conjunction with the sampling configuration. The prior was randomly distributed between 40 and 600 days. While differential evolution and snooker algorithms were created in an attempt to overcome the problem of walkers converging on local optima, the probability distribution of this parameter space make random walks of that magnitude and specificity unlikely. As such, while the 173 day model fits the data more appropriately, the 346 day model was the favored by the probability distribution and mcmc configuration.



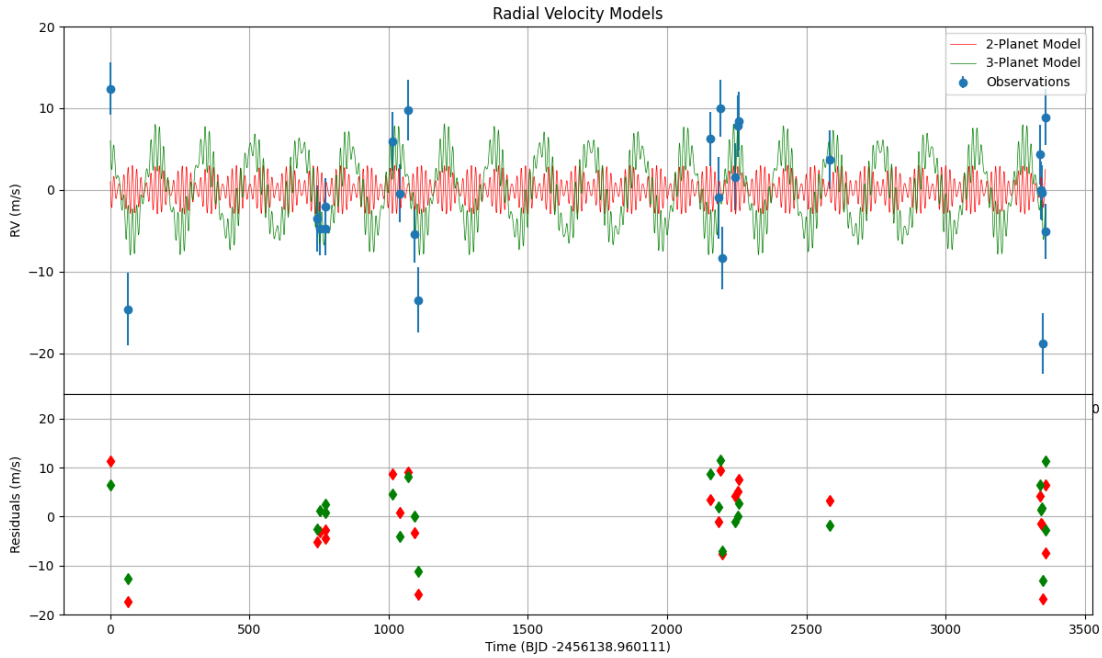


Figure 5.1: Radial velocity simulations of Kepler-36 induced by each of my best-fit models. Observations are shown as blue dots. Residuals are shown in the lower panel.

Because a third body has little impact on the the observed transit timing variations the constraints on this body are primarily informed by the RV measurements. As established, this data alone is not sufficient to constrain the posterior distribution with more specificity than these modes.

The highest likelihood, best-fit orbital elements were used for all subsequent post-fit analyses. Figure 4.3 illustrates the TTVs experienced by the two inner planets in each simulation, which are in good approximation to those deduced from *Kepler* data as well as to each opposing simulation. The simulated RVs, along with residuals, are shown in Figure 5.1. Keeping in mind that my best-fit two-planet model is comparable to previous studies of this system, this figure also helps to highlight the discrepancy between the currently accepted configuration of the Kepler-36 system and the RV behavior of the host star as measured by HIRES.

As discussed previously, Figure 5.2 shows the periodogram of the residuals of the RV data as

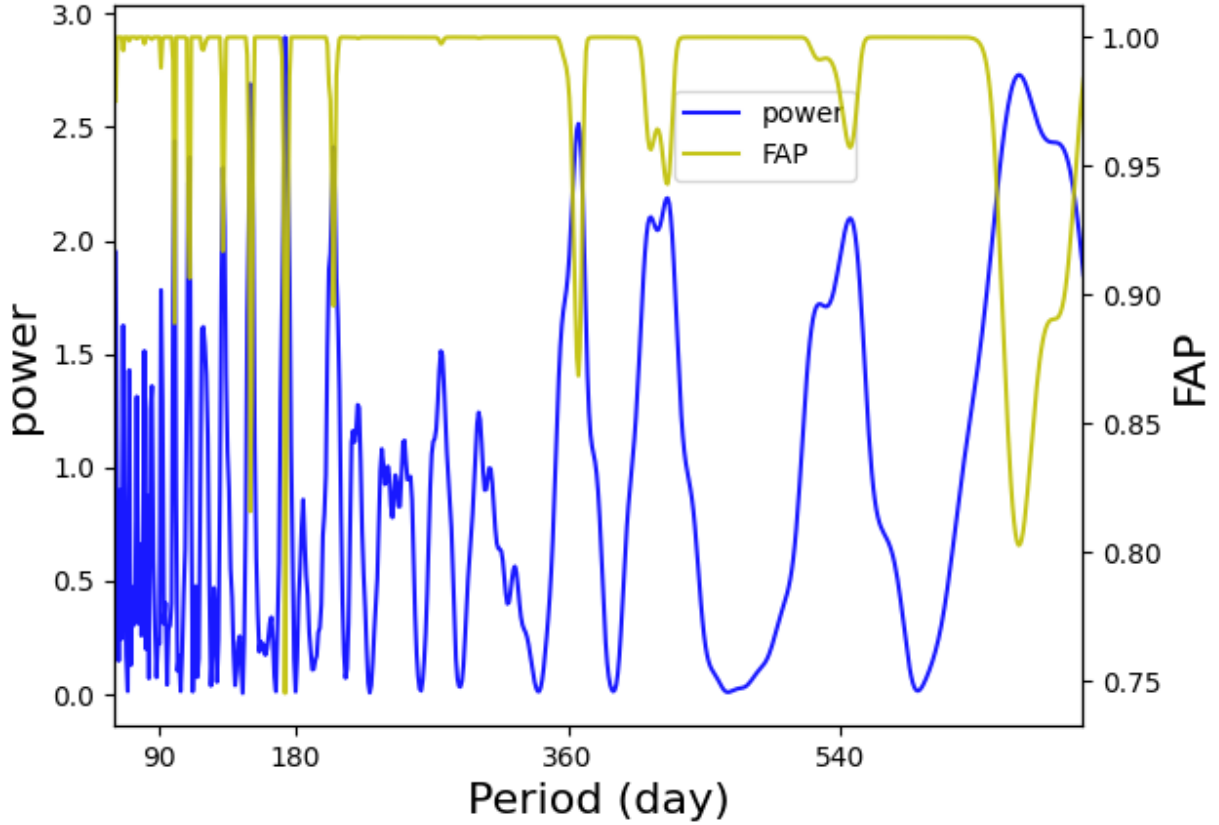


Figure 5.2: The Lomb-Scargle periodogram of the residuals of the RV data as simulated by the posterior maximum likelihood orbital elements of the two-planet fit. The yellow line denotes the false alarm probability.

simulated by the posterior maximum likelihood of the two-planet model. Note that the maximal peak of this periodogram is  $\sim 173$  days. While I intentionally ignored this value when establishing the priors for my three-planet fit, it is further supported by the posterior distribution of the three-planet model. In other words, the periodogram of the residuals of the RV simulation of the two-planet model has a maximal peak that matches the fitted orbital period of the third planet of the three-planet model. These matching values are obtained independently of each other.

Table 5.1: The standard deviation of the posterior distribution of each parameter in the two-planet fit

Orbital Element	Standard Deviation	Prior Range	% of Prior
$m_b$	0.0674	9	0.75%
$P_b$	0.000246	0.1	0.25%
$e_b$	0.00208	0.04	5.20%
$w_b$	2.855	360	0.79%
$M_b$	2.695	360	0.75%
$m_c$	0.0754	9	0.84%
$P_c$	0.0001675	0.1	0.17%
$e_c$	0.001425	0.04	3.56%
$w_c$	30.65	360	8.51%
$M_c$	30.7	360	8.53%

Table 5.2: The standard deviation of the posterior distribution of each parameter in the three-planet fit

Orbital Element	Standard Deviation	Prior Range	% of Prior
$m_b$	0.052	9	0.58%
$P_b$	0.00028	0.1	0.28%
$e_b$	0.0024	0.04	6.00%
$\omega_b$	4.52	360	1.26%
$M_b$	4.27	360	1.19%
$m_c$	0.0746	9	0.83%
$P_c$	0.00158	0.1	1.58%
$e_c$	0.00255	0.04	6.38%
$\omega_c$	13.9	360	3.86%
$M_c$	13.85	360	3.85%
$m_d$	13.1	399	3.28%
$P_d$	77.26	560	13.80%
$M_d$	46.85	360	13.01%

## 5.2 Statistical Analysis

After obtaining models with the highest likelihood from my fits and simulating observations based on these models, I then sought to assess the statistical significance of these models. The primary criteria I rely on to assess the quality of my fits are the  $\chi^2$  test and the Bayesian Information Criterion (BIC). Both tests are useful in this assessment because they do not consider how the models were obtained. They simply provide vetting tools for the models themselves in the context of observational data.

As described in Andrae et al. (2010), the  $\chi^2_{red}$  test can be used as an assessment of the "goodness of fit" of a model as well as provide a comparison of multiple models to each other.  $\chi^2$  is calculated using the following equation.

$$\chi^2 = \sum_{n=1}^{\infty} \left( \frac{y_n - f(\vec{x}_n; \vec{\theta})}{\sigma_n} \right)^2 \quad (5.1)$$

This value is then standardized, or "reduced," by

$$\chi^2_{red} = \frac{\chi^2}{k} \quad (5.2)$$

where  $K$  is the number of degrees of freedom. When given data and multiple models, this test helps assess which model fits the data best. The better fitting model is the one whose  $\chi^2_{red}$  value is closest to one. Taken further, the  $\chi^2_{red}$  may be applied to single-model assessment. In this context,  $\chi^2_{red} > 1$  signifies an incomplete fit and  $\chi^2_{red} < 1$  denotes an overfit.

Applying the  $\chi^2_{red}$  test to my best-fit models for each configuration demonstrates favorability toward the three-planet system. Corresponding values are recorded in table 5.3. Since  $\Delta\chi^2_{red}$  is

Table 5.3: Statistical test results

	Reduced $\chi^2$	Bayesian Information Criterion
Two-Planet Model	8.05	710.62
Three-Planet Model	3.36	692.13
$\Delta$	4.59	18.49

4.59 in favor of the three-planet model and the  $\chi^2_{red}$  of the three-planet model is closer to one, this model is the more likely explanation of the HIRES observations. It is, however, still an incomplete explanation of the observations since the  $\chi^2_{red}$  of the three-planet model is greater than one. An alternate explanation of this  $\chi^2_{red}$  could be underestimated RV uncertainties.

I can further support my claim using the BIC, given as

$$BIC = k \ln n - 2 \ln \hat{L} \quad (5.3)$$

where  $k$  is the number of free parameters (non-fixed orbital elements) estimated by the model,  $n$  is the number of observations, and  $\hat{L}$  is the maximized value of the likelihood function of the model. Models with a lower BIC are preferred. Using the Jeffreys' scale as described in Liddle (2007), I treat  $\Delta BIC > 10$  as decisive evidence in favor of the model with the lower information criterion.

In this case, the three-planet model has a lower BIC (692.13) than the two-planet model (710.62). This  $\Delta BIC$  (18.49) also provides decisive support for the case for the three-planet model.

## CHAPTER 6 DISCUSSION

My analysis described above justifies the candidacy of an additional body in the Kepler-36 system. Leveraging the additional information of RV measurements, I have completed DEMCMC fits for the current two-planet model and an expanded three-planet model using priors both uninformative and bound by physically viable constraints. These fits generated models that are in agreement with the current configuration of this system. The three-planet model more accurately simulates the TTV and RV measurements available to us. Moreover, commonly accepted statistical tools provide further justification for the adoption of this three-planet model.

However, additional observations should be made. It is clear that this three-planet model, while compelling, fails to fully explain the dynamics of this system. This claim is most obviously supported by the fact that the fit did not isolate the posterior to a single orbital period. HIRES data provided significant assistance in further constraining the behavior of this planetary system, but sampling cadence and quantity problems persist. Efforts to fit a fourth orbiting body in this research were futile, as the penalty that came with a more complex simulation were not able to be overcome by the improvement in fit. Intuitive interpretation of my results lead to the understanding that there is more activity in this system than even a three-planet model can explain. As such, future efforts to explain the discrepancy between current models and observations will require even more data.

The values of the bimodal peaks of  $P_d$  at approximately 173 and 346 days are of note. In addition to being close to the periodicity of the ground-based Kepler field observing season and

its alias, they are in proximity to the Earth's orbital period. I have not attempted to explore the possibility of this signal being an alias for either of these cadences and instead choose defer this exploration to future efforts that possess the requisite additional data. Future iterations of this effort could also independently explore each of these peaks and compare their fit to the data.

As discussed above, explanations for the formation of the Kepler-36 system are abundant and inconclusive (Quillen et al. 2013; Paardekooper et al. 2013; Bodenheimer et al. 2018; Rimlinger & Hamilton 2020). Early scenarios favored formation via migration. More recent works have been able to model the known two-planet system with both migration and in situ approaches. Coupled with the vastly differing densities and orbital proximity of the two known planets, the inclusion of a longer period planet in this system could pose a significant challenge.

In the case of migration models, the need to account for a higher mass, longer period planet would necessitate modified constraints the initial conditions of these models in the interest of orbital stability. Furthermore, these models would need to sufficiently account for varying migration rates or magnitudes such that two short period orbits and at least one longer period orbit could be observed today.

In situ models would be affected primarily at the accretion phase, where another body would affect impact the configuration of feeding materials. This third body would itself accrete feeding material, providing further constraints on the range and amount of material initially available to the two known planets than previous studies have considered.

## REFERENCES

- Agol, E. & Carter, J. A. 2019
- Andrae, R., Schulze-Hartung, T., & Melchior, P. 2010, Dos and don'ts of reduced chi-squared
- Bodenheimer, P., Stevenson, D. J., Lissauer, J. J., & D'Angelo, G. 2018
- Braak, C. J. F. T. 2006, *Statistics and Computing*, 16, 239
- Carter, J. A., Agol, E., Chaplin, W. J., Basu, S., Bedding, T. R., Buchhave, L. A., Christensen-Dalsgaard, J., Deck, K. M., Elsworth, Y., Fabrycky, D. C., Ford, E. B., Fortney, J. J., Hale, S. J., Handberg, R., Hekker, S., Holman, M. J., Huber, D., Karoff, C., Kawaler, S. D., Kjeldsen, H., Lissauer, J. J., Lopez, E. D., Lund, M. N., Lundkvist, M., Metcalfe, T. S., Miglio, A., Rogers, L. A., Stello, D., Borucki, W. J., Bryson, S., Christiansen, J. L., Cochran, W. D., Geary, J. C., Gilliland, R. L., Haas, M. R., Hall, J., Howard, A. W., Jenkins, J. M., Klaus, T., Koch, D. G., Latham, D. W., MacQueen, P. J., Sasselov, D., Steffen, J. H., Twicken, J. D., & Winn, J. N. 2012, *Science*, 337, 556
- Coughlin, J. L., Mullally, F., Thompson, S. E., Rowe, J. F., Burke, C. J., Latham, D. W., Batalha, N. M., Ofir, A., Quarles, B. L., Henze, C. E., Wolfgang, A., Caldwell, D. A., Bryson, S. T., Shporer, A., Catanzarite, J., Akeson, R., Barclay, T., Borucki, W. J., Boyajian, T. S., Campbell, J. R., Christiansen, J. L., Girouard, F. R., Haas, M. R., Howell, S. B., Huber, D., Jenkins, J. M., Li, J., Patil-Sabale, A., Quintana, E. V., Ramirez, S., Seader, S., Smith, J. C., Tenenbaum, P., Twicken, J. D., & Zamudio, K. A. 2015
- Deck, K. M., Agol, E., Holman, M. J., & Nesvorný, D. 2014, *ApJ*, 787, 132



- Deck, K. M., Holman, M. J., Agol, E., Carter, J. A., Lissauer, J. J., Ragozzine, D., & Winn, J. N. 2012, *The Astrophysical Journal*, 755, L21
- Foreman-Mackey, D., Hogg, D. W., Lang, D., & Goodman, J. 2012
- Gelman, A. & Rubin, D. B. 1992, *Statistical Science*, 7, 457
- Goodman, J. & Weare, J. 2010, *Communications in Applied Mathematics and Computational Science*, 5, 65
- Hadden, S. & Lithwick, Y. 2017, *AJ*, 154, 5
- Jontof-Hutter, D., Wolfgang, A., Ford, E. B., Lissauer, J. J., Fabrycky, D. C., & Rowe, J. F. 2021
- Liddle, A. R. 2007
- Lopez, E. & Fortney, J. 2013
- Morton, T. D., Bryson, S. T., Coughlin, J. L., Rowe, J. F., Ravichandran, G., Petigura, E. A., Haas, M. R., & Batalha, N. M. 2016
- Nesvorny, D. & Vokrouhlicky, D. 2014
- Paardekooper, S.-J., Rein, H., & Kley, W. 2013
- Quillen, A. C., Bodman, E., & Moore, A. 2013
- Rimlinger, T. & Hamilton, D. 2020, *Monthly Notices of the Royal Astronomical Society*, 501, 4255
- Rowe, J. F., Coughlin, J. L., Antoci, V., Barclay, T., Batalha, N. M., Borucki, W. J., Burke, C. J., Bryson, S. T., Caldwell, D. A., Campbell, J. R., Catanzarite, J. H., Christiansen, J. L., Cochran, W., Gilliland, R. L., Girouard, F. R., Haas, M. R., Helminiak, K. G., Henze, C. E., Hoffman, K. L., Howell, S. B., Huber, D., Hunter, R. C., Jang-Condell, H., Jenkins, J. M., Klaus, T. C., Latham, D. W., Li, J., Lissauer, J. J., McCauliff, S. D., Morris, R. L., Mullally, F., Ofir, A., Quarles, B., Quintana, E., Sabale, A., Seader, S., Shporer, A., Smith, J. C., Steffen, J. H., Still,

- M., Tenenbaum, P., Thompson, S. E., Twicken, J. D., Van Laerhoven, C., Wolfgang, A., & Zamudio, K. A. 2015, ApJS, 217, 16
- ter Braak, C. J. F. & Vrugt, J. A. 2008, Statistics and Computing, 18, 435
- Vissapragada, S., Jontof-Hutter, D., Shporer, A., Knutson, H. A., Liu, L., Thorngren, D., Lee, E. J., Chachan, Y., Mawet, D., Millar-Blanchaer, M. A., Nilsson, R., Tinyanont, S., Vasisht, G., & Wright, J. 2019
- Yoffe, G., Ofir, A., & Aharonson, O. 2020

## CURRICULUM VITAE

Nicholas J. Juliano

Department of Physics and Astronomy  
University of Nevada, Las Vegas  
4505 S. Maryland Pkwy  
Las Vegas, NV 89154-4002  
nicholasjosephjuliano@gmail.com

### EDUCATION

**State University of New York at Oneonta**  
B.S., Physics (astronomy concentration), 2011

### EXPERIENCE

**General Atomics - CCRi**, Charlottesville, VA  
Data Scientist, June 2022–current

**Hamilton Planetarium Scholarship**, Las Vegas, NV  
Trustee, October 2019–June 2022

**University of Nevada, Las Vegas**, Las Vegas, NV  
Graduate Research Assistant for Jason Steffen, Fall 2019–current  
Jason Steffen Research Group, Fall 2019–current

**CHOLLA Informal Education Consortium**, Las Vegas, NV  
Chair of Outreach, May 2019–September 2020  
Webmaster, May 2017–June 2022  
Member, August 2016–June 2022

**The College of Southern Nevada**, Las Vegas, NV Adjunct Instructor, January 2017–May 2018  
Planetarium Program Manager, August 2016–June 2022

**The Newark Museum**, Newark, NJ  
Planetarium Educator, February 2015–November 2015  
Intern, May 2014–February 2015

**State University of New York at Oneonta**, Oneonta, NY  
Physics Tutor, September 2014–February 2015  
OnMark Marketing Club VP of Special Projects, May 2014–May 2015

Physics Club Secretary, May 2013–May 2014  
Planetarium & Observatory Assistant, August 2011–May 2015

## SKILLS

**Languages:** Python, Docker, Kubernetes, Matlab, HTML, Markdown, SQL, CSS

**Analytical Methods:** Neural Networks, Bayesian Statistics, Fourier Analysis, Model Selection, Bootstrap Analysis, Data Visualization

**Operating/Software Systems:** Mac OS, Windows, Linux, Latex, Git, Power BI, Tableau, Workable

**Technologies/Protocols/Frameworks:** Technologies/Protocols/Frameworks: SSH, PBS, Documentation, Jupyter Notebook, Docker, Kubernetes, Cuda

## GRANTS, SCHOLARSHIPS, AND AWARDS

- Hamilton Planetarium Scholarship, 2014
- State University of New York at Oneonta Research Grant, 2013
- GCSANJ Scholarship, 2011 & 2013
- GCSAA Scholarship, 2011
- Theodore J. Ryken Chapter of the National Honors Society, 2011

## TEACHING

**University of Nevada, Las Vegas**

Teaching Assistant, Department of Physics and Astronomy, Fall 2019–Spring 2022

**College of Southern Nevada**

Adjunct Instructor, Introductory Astronomy Laboratory, Spring 2017–Spring 2018

## PRESENTATIONS

- **Poster** Exoplanets IV, May 2022, *Constraints on the Kepler-36 System from Transit Timing Variations and New Radial Velocity Data*
- **Seminar** SUNY Oneonta Department of Physics and Astronomy Career Series, Apr. 2022, *Kinematics and Dynamics: How the Trajectory of Life can Fail to Obey Introductory Physical Principles and how Exoplanets Cannot*
- **Keynote** Las Vegas Astronomical Society Meeting, Mar. 2022, *The Complicated Process of Simplifying: Automating Astronomy*
- **Presentation** Rotary Club of North Las Vegas Meeting, Aug. 2018, *The College of Southern Nevada Planetarium*
- **Poster** SUNY Oneonta Student Research and Creativity Day, Apr. 2015, *Utilizing the SUNY Oneonta Planetarium for Scientific Education*

- **Poster** SUNY Oneonta Student Research and Creativity Day, Mar. 2014, *Constructing and Utilizing a Flat-Field Calibration Device for Astronomical Image Correction*